ACTA IMEKO
ISSN: 2221-870X
September 2024, Volume 13, Number 3, 1 - 8

Bearing fault detection using second-order moment spectrum and adaptive time-varying morphological filtering

Karim Bouaouiche[1], Yamina Menasria[1], Dalila Khalfa[1], Teyar Soumia[2], Gheribi Hassina[2]

[1] *Electromechanical Engineering Laboratory, Electromechanical Department, Faculty of Technology, Badji Mokhtar-Annaba University, P.O.Box 12, Annaba, 23000, Algeria*
[2] *Mechanical Engineering Department, Faculty of Technology, University of 20 August 1955 Skikda, BP 26 Skikda 21000, Algeria*

ABSTRACT
The second-order moment spectrum is a method designed to simplify the complex shape of the spectrum, thus facilitating its interpretation for the identification and localization of defects based on peak frequency. Generally used as a final step in defect detection methods, this method offers the advantage of a more easily interpretable spectral shape. Compared to the shape of the spectrum of the vibration signal defined by the Fourier transform, which includes sidebands composed of peaks of large amplitude at different frequencies, the spectrum generated by the second-order moment spectrum method stands out for its simplicity. Starting from the mean and standard deviation of the vibration signal, the second-order moment can be defined as the power of the ratio between the standard deviation and the difference between the signal and the mean. Next, the Fourier transform is applied to express the second-order moment spectrum. The performance of the second-order moment spectrum is evaluated using the principle of comparison with the envelope spectrum obtained by the Hilbert transform. Vibration signals are analyzed using two methods: adaptive time-varying morphological filtering and second-order moment spectrum. After applying these methods to the signals from the database, we observe high-amplitude peaks at the frequencies corresponding to inner ring and ball defects. The second-order moment spectrum gives similar results to those obtained with the Hilbert transform envelope.

Section: RESEARCH PAPER

Keywords: Bearing; vibration signal; second-order moment; defect detection

Citation: K. Bouaouiche, Y. Menasria, D. Khalfa, S. Teyar, H. Gheribi, Bearing fault detection using second-order moment spectrum and adaptive time-varying morphological filtering, Acta IMEKO, vol. 13 (2024) no. 3, pp. 1-8. DOI: 10.21014/actaimeko.v13i3.1707

Section Editor: Laura Fabbiano, Politecnico di Bari, Italy

Received November 10, 2024; **In final form** July 26, 2024; **Published** September 2024

Funding: This work was supported by electromechanical engineering laboratory, Algeria.

Corresponding author: Karim Bouaouiche, e-mail: karim.bouaouiche@univ-annaba.dz

1. INTRODUCTION

Bearings are components located inside rotating machinery, typically consisting of an inner ring, an outer ring, a cage, and rolling elements [1]. They play a crucial role in facilitating the conversion of motion between shafts, and any failure causes such as fatigue, wear, corrosion, or deformation result in a reduction in the reliability of rotating machinery [1]. Bearing causes 40-45% of defects inside electrical machinery such as motors [2]. Additionally, various fault detection techniques are utilized, including oil analysis, temperature analysis, acoustic analysis, and vibration analysis [2]. However, in the industrial environment, vibration analysis is the most effective technique, since vibration signals contain information about the defects present inside the machine and depend on the rotating part [2], [3]. In addition, vibration analysis can be performed without disassembling the machine components, unlike oil analysis, which requires some disassembly [2], [3]. Similarly, the application of sound signals used in acoustic analysis for accurate measurements requires an isolated measurement environment to avoid other sound sources from nearby machines [2], [3]. After discussing the importance of bearings and the prevalence of faults, vibration signal analysis involves two crucial steps. The first step involves gathering the signals using a measurement chain equipped with sensors like accelerometers, while the other step is related to signal processing using methods that incorporate mathematical and computational tools [4].

The processing of vibration signals is an interdisciplinary field that encompasses various signal analysis methods for fault detection [5]. Among these methods, some involve decomposing the vibration signal into multiple simpler signals and

subsequently performing a selection operation on the signal that is most sensitive to defects, using indicators [5]. This approach subsequently enables the reconstruction of an additional signal that includes information regarding anomalies [5]. The decomposition of signals is performed using algorithms such as successive variational mode decomposition [6], variational mode extraction [7], and empirical Fourier decomposition [8]. As for the selection indicators, we find kurtosis [4], correlation [2], the Gini index [9], and weighted entropy index [10].

Furthermore, signal demodulation techniques are commonly employed as a final step to extract and localize the faulty component by comparing the theoretical values of fault frequencies with the frequency of peaks in the spectra [4]. Two methods are particularly popular for signal demodulation, namely the Hilbert transform [11] and the Teager-Kaiser energy operator [12]. Therefore, the fault frequencies of bearing components are determined based on geometric parameters and rotation speed [2]. Furthermore, information regarding defects can be defined based on the selection of effective frequency bands using the kurtogram method, which relies on the representation of spectral kurtosis as a function of frequency [13], or through the use of a candidate fault frequencies gram (CFFsgram) [14].

Vibration signals consist of an impulsive part and a noisy part correlated with each other by a convolution product [15]. The defect information is usually in the impulse part [15]. Thus, the separation between these two parts plays a crucial role in diagnosis [15]. The various methods considered for extracting the impulse part are based on the inverse process of convolution, known as deconvolution [15]. In this context, there are signal deconvolution methods such as Minimum Entropy Deconvolution [16], Maximum Correlated Kurtosis Deconvolution [17], Maximum Cyclostationarity Deconvolution [18], and Adaptive Maximum Cyclostationarity Blind Deconvolution [19]. Furthermore, machine learning and deep learning methods are integrated into defect detection [20]. The general principle of these methods focuses on proposing new features determined in the time or frequency domain of the signals from the faulty and healthy states of the bearing [20]. Next, classifiers are employed to categorize the feature values and determine the type of defect. Several classifiers are used in diagnostics, such as Support Vector Machine, K-nearest neighbour, Artificial Neural Network, Convolutional Neural Network [20].

In this paper, we propose an approach for detecting bearing defects. Second-Order Moment Spectrum (SOMS) and Adaptive Time-Varying Morphological Filtering (ATVMF) are two methods integrated into the approach, with ATVMF designed to eliminate noise and extract defect-related pulses from the signals. Additionally, the second-order moment spectrum is created to locate the defect based on the peak frequency.

2. METHODS

2.1. Defect Detection Method

Figure 1 presents the method for detecting bearing defects, developed by us and composed of two steps:

1. Step 1: Adaptive Time-Varying Morphological Filtering (ATVMF) is applied to the vibration signal to eliminate noise and extract the impulse part of the signal.
2. Step 2: determination of the Second-Order Moment Spectrum (SOMS) to locate the faulty component in the bearing. The comparison between the peak frequencies of SOMS and the defect frequencies of the bearing elements allows for the detection of defects. The defect frequencies of the bearing are defined by the following formulas [2]:

- Inner race fault frequency (IRFF):

$$IRFF = \frac{z \times Fr}{2}\left(1 + \frac{d}{Dm}\cos(a)\right), \quad (1)$$

- Outer race fault frequency (ORFF):

$$ORFF = \frac{z \times Fr}{2}\left(1 - \frac{d}{Dm}\cos(a)\right), \quad (2)$$

- Ball fault frequency (BFF):

$$BFF = \frac{Dm \times Fr}{2d}\left(1 - \left(\frac{d}{Dm}\cos(a)\right)^2\right), \quad (3)$$

- Cage fault frequency (CFF):

$$CFF = \frac{Fr}{2}\left(1 - \frac{d}{Dm}\cos(a)\right), \quad (4)$$

with z: number of balls, Fr: operating speed, a: angle of contact, d: diameter of ball, Dm: pitch diameter.

The proposed method is implemented using MATLAB software, with a program that encompasses all the steps outlined in the method flowchart (Figure 1).

2.2. Adaptive time-varying morphological filtering

Adaptive time-varying morphological filtering (ATVMF) is a method involving the use of structuring elements and

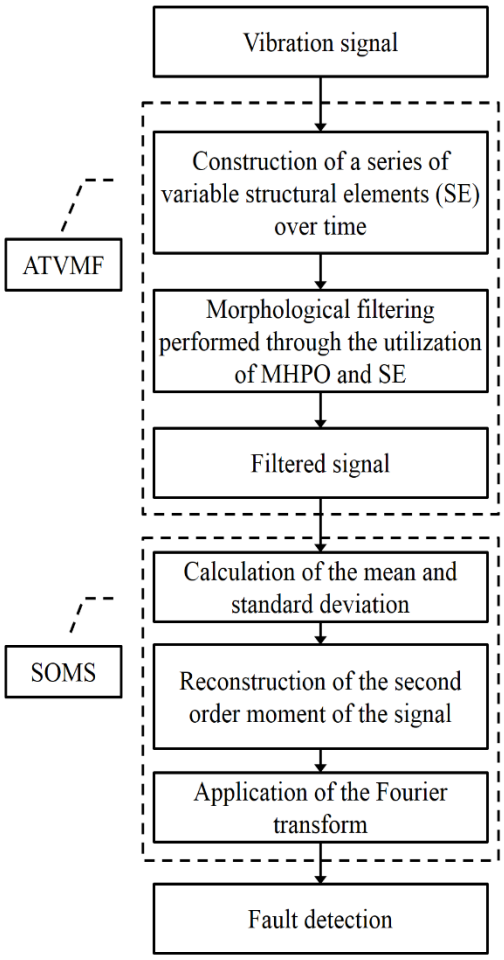

Figure 1. Defect detection method.

morphological operators to eliminate noise and extract pulse information, and provides a highly efficient filtering operation for signals [21]. The ATVMF method consists of the following two steps [21]:

1. Formulation of a series of time-varying structural elements (SE) based on the signal. The structural elements are established after identifying all the signal's minimum and maximum points, and interpolation methods are then employed to obtain a new sequence. The alignment between two minimum points in the result of the interpolation method is considered as a structural element.
2. Morphological filtering is applied to the signal using the morphology hat product operation (*MHPO*), *MHPO1*, or *MHPO2* operators. The equations below define these operators.

$$MHPO(n) = AHCO(n) \times AHCOOC(n)\,, \tag{5}$$

$$MHPO1(n) = AHDE(n) \times AHCO(n)\,, \tag{6}$$

$$MHPO2(n) = AHDE(n) \times AHCOOC(n)\,, \tag{7}$$

with *AHCO*: closing and opening average-hat operator, *AHCOOC*: closing-opening and opening-closing average-hat operator, *AHDE*: dilation and erosion average hat operator.

Two input parameters for the ATVMF method include the interpolation method type and the chosen morphological operator.

2.3. Second order moment spectrum

The second-order moment spectrum (SOMS) is a method used to simplify the complex shape of vibration signal spectra, making their interpretation easier. The random distribution of peak shapes reflects the complexity, whereas simplicity is expressed through the variation of organized peaks. By using Fourier transform, the mean, and the standard deviation of the signal, the second-order moment spectrum is formulated through the following steps:

- Calculation of the mean and standard deviation of the vibration signal (x(t)) using the following two equations:

$$\bar{x} = \frac{1}{L}\left(\sum_{i=1}^{L} x_i\right), \tag{8}$$

$$std(x) = \sqrt{\frac{\sum_{i=1}^{L}(x_i - \bar{x})^2}{L}}\,, \tag{9}$$

- The reconstruction of the second order moment of the signal is done using the proposed formula:

$$som(t) = \frac{1}{L}\left(\frac{x(t) - \bar{x}}{std(x)}\right)^2\,, \tag{10}$$

- Applying the Fourier transform to $som(t)$ to obtain the second order moment spectrum.

$$soms(f) = \int_{-\infty}^{+\infty} som(t)\, e^{-j\,2\,\pi\,f\,t} dt\,. \tag{11}$$

Evaluation of second-order moment spectrum performance

The performance evaluation of the second order moment spectrum is done by comparing the frequencies of peaks observed in the SOMS with the envelope spectrum obtained using the Hilbert transform. Subsequently, classification between the SOMS and the envelope spectrum obtained through the Hilbert transform is performed based on the features. The following equations represent the envelope spectrum obtained through the Hilbert transform [4]:

$$H[x(t)] = x(t) * \frac{1}{\pi\, t}\,, \tag{12}$$

$$A(t) = x(t) + j\, H[x(t)]\,, \tag{13}$$

$$E_n(t) = \sqrt{x(t)^2 + H[x(t)]^2}\,, \tag{14}$$

$$E_n(f) = \mathrm{FFT}(E_n(t)), \tag{15}$$

H: Hilbert transform, *: product convolution, E_n: envelope, FFT: fast Fourier transform.

Demodulating signals using the Hilbert transform is chosen to evaluate the performance of SOMS because it is very useful in diagnostics as a final step for detecting faulty components based on peak frequency. Table 1 presents the features used to generate a matrix appearing in (16)

$$\boldsymbol{C} = [max, min, rms, \ldots\ldots\ldots, mean]\,. \tag{16}$$

The matrix (*C*) comprises the features of the second-order moment spectrum (SOMS) and the envelope spectrum. After determining this matrix, we proceed to divide the data into 80% training data to train the support vector machine (SVM) classifier and 20% test data to validate the classifier. Next, we establish two classes: (1) for the second-order moment spectrum and (-1)

Table 1. Features.

Features	Formulas
Maximum	$\max(x_i)$
Minimum	$\min(x_i)$
Root mean square (rms)	$\sqrt{\frac{1}{L}\sum_{i=1}^{L} {x_i}^2}$
Skewness	$\frac{1}{(L-1)(L-2)}\left(\frac{x_i - \bar{x}}{std(x)}\right)^3$
Kurtosis	$\frac{1}{L}\sum_{i=1}^{L}\left(\frac{x_i - \bar{x}}{std(x)}\right)^4$
Variance	$\frac{1}{L}\sum_{i=1}^{L}(x_i - \bar{x})^2$
Standard deviation (std)	$\sqrt{\frac{\sum_{i=1}^{L}(x_i - \bar{x})^2}{L}}$
Creast factor	$\frac{rms}{max}$
Median	$\mathrm{median}(x_i)$
Sum	$\sum_{i=1}^{L} x_i$
Mean	$\frac{1}{L}\sum_{i=1}^{L} x_i$

for the envelope spectrum, determined by the Hilbert transformation. Finally, we obtain a classification of the method types.

The principle of SVM is based on constructing a hyperplane to separate two different types of samples while considering the minimization of structural risk [22]. The hyperplane is expressed by equation (17) [23].

$$f(x) = W^{\mathrm{T}} + b, \quad (17)$$

(x): represents the input data, the position of the hyperplane is determined by the vector (W) and the scalar (b), and through the application of the sign function on ($f(x)$), the samples are classified into positive or negative classes [23]. In addition, non-linear classification by support vector machine incorporates the use of kernel functions [23]. The performance of the SVM classifier is defined by equation (18), which has been determined from the confusion matrix [24].

$$a = \frac{Number\ of\ correctly\ classified\ samples}{Total\ number\ of\ samples} \times 100, \quad (18)$$

3. EXPERIMENTAL STUDY

3.1. CWRU database

In this subsection, we analyse the vibration signals resulting from a defect in the inner ring of a ball bearing of the type 6205-2 RS JEM SKF [25]. This bearing is located at the end of an electric motor on the driver side, as shown in the test strip used in the Case Western Reserve University (CWRU) database [25]. The signals measured by accelerometers are recorded as MATLAB files with a sampling frequency of 48 kHz [25]. During the test, the operating conditions, load, speed, and the diameter of the defect in the inner ring of the bearing are varied [25]. Equation (19) expresses the inner ring defect frequency [25].

$$IRFF = 5.4152 \times Fr, \quad (19)$$

Table 2 contains the vibration signals from the inner ring defect with a diameter of 0.5334 mm. Two vibration signals, each comprising 48000 samples, are analysed by the proposed method, as shown in Table 2, along with the sampling frequency.

Results and discussions

For signal 1, after applying the method (Figure 1), we observe a significant peak at the inner ring defect frequency of the bearing in the second-order moment spectrum (161.9 Hz ≅ 162.18 Hz), as shown in Figure 2.

A high amplitude is observed in the inner ring defect frequency of the bearing in the second-order moment spectrum of signal 2 (159.7 Hz≅159.92 Hz), as shown in the Figure 3.

Performance of the second-order moment spectrum: the envelope spectrum of the Hilbert transform indicates the same results as those obtained by the SOMS method, as shown in Figure 4 and Figure 5. In this case, the second-order moment spectrum illustrates a good result.

Table 2. Vibration signals.

Signals	Fault frequency Hz	Speed RPM	Load N · m / s
Signal1: X213_DE_time	162.18	1797	0
Signal2: X214_DE_time	159.92	1772	745.6

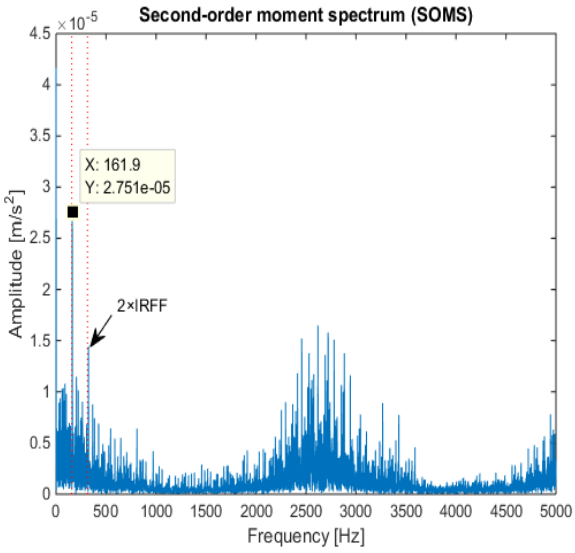

Figure 2. SOMS of signal 1.

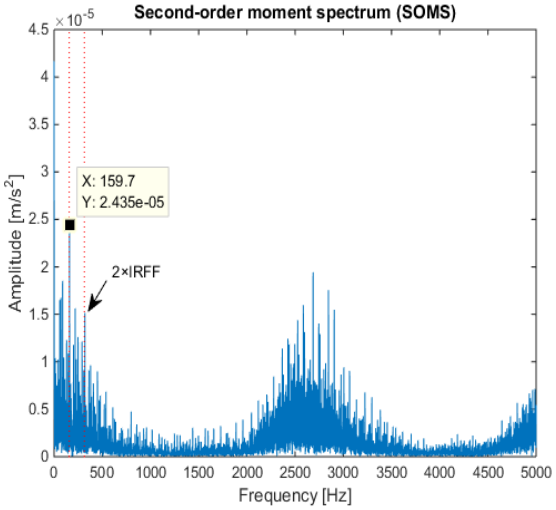

Figure 3. SOMS of signal 2.

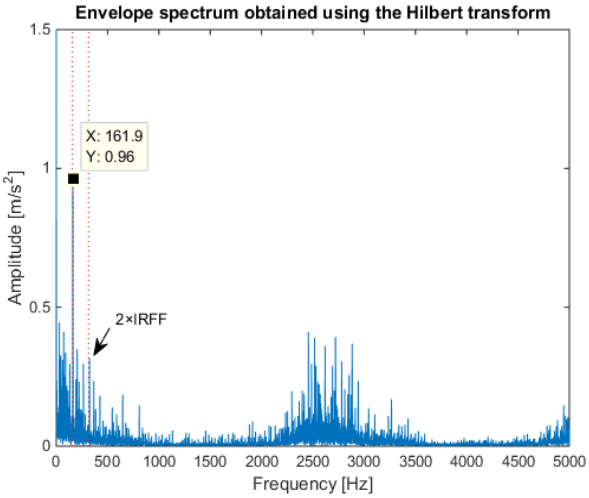

Figure 4. Envelope spectrum of signal 1

The feature values are calculated from the second-order moment spectrum and the envelope spectrum obtained by the Hilbert transform of the two previously analysed signals,

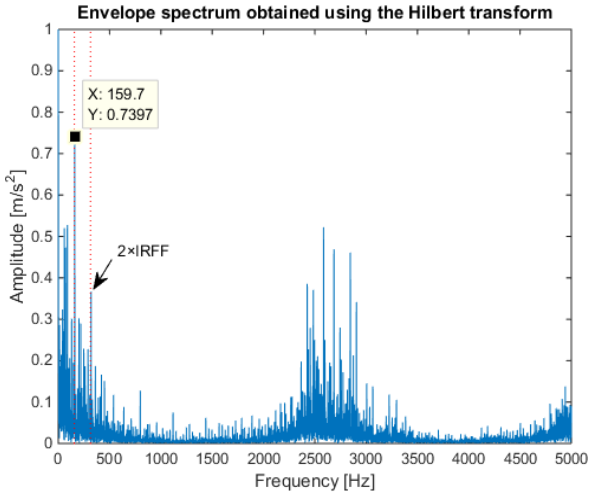

Figure 5. Envelope spectrum of signal 2.

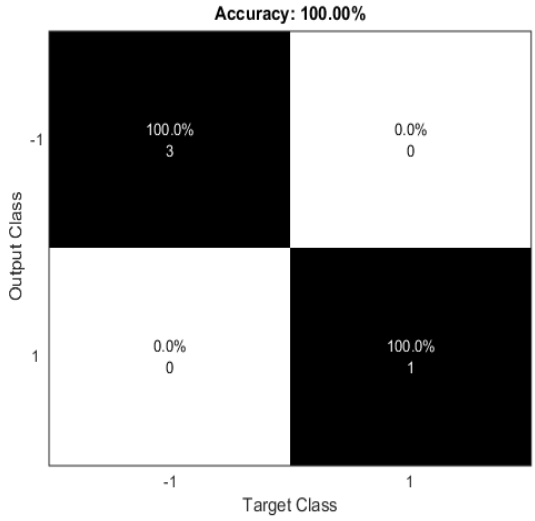

Figure 6. Confusion matrix.

allowing the construction of matrix (C). When the SVM method is applied, a high performance of 100% is obtained, as shown in the confusion matrix (Figure 6), with the actual classes on the Y-axis and the predicted classes on the X-axis.

Classes 1 represent SOMS, and -1 represents the envelope spectrum determined by the Hilbert transform. Furthermore, the diagonal represents the prediction performances. The features mentioned in Table 1 effectively enable the selection of the method type.

3.2. HUST database

This database includes fault signals from several bearings identified under the symbols 6204, 6205, 6206, 6207, and 6208 [20]. All faults appear in the form of microcracks with a width of 0.2 mm created using the wire cutting method. The test strip used in the Hanoi University of Science and Technology (HUST) database includes a 1 HP electric motor controlled by an inverter and a powder brake, as well as a PCB 325C33 accelerometer positioned in the bearing housing [20]. Additionally, a torque sensor is used on the dynamometer to monitor the load and speed [20]. The acceleration of bearing vibrations is recorded in the form of MATLAB files with a sampling frequency of 51.2 kHz [20]. We will select two signals from bearings 6206 and 6208 to validate the effectiveness of the proposed method. Therefore, the length of each signal is 51200 samples.

Table 3. Vibration signals for analysis.

Bearings	Signals	Speed Hz	Load W	Fault frequency Hz	Defect component
6206	B604	22.7	400	*Fd* = 111.57	Ball
6208	B804	22.84	400	*FD* = 109.63	Ball

Results

The second-order moment spectrum of signal B804 displays a series of peaks at the ball defect frequency (110.2 Hz ≅ *FD*), with a decrease in vibration acceleration amplitude as a function of frequency, as shown in the Figure 7.

A high-amplitude peak is present at the ball defect frequency (107 Hz ≅ *Fd*), as indicated by the second-order moment spectrum of signal B604 (Figure 8).

Comparison between the results: the envelope spectrum of the analysed signals yields the same result as that found by SOMS, as shown in Figure 9 and Figure 10. Furthermore, the amplitude decreases as the frequency increases, thereby allowing for the detection and localization of the defect based on the peak frequencies.

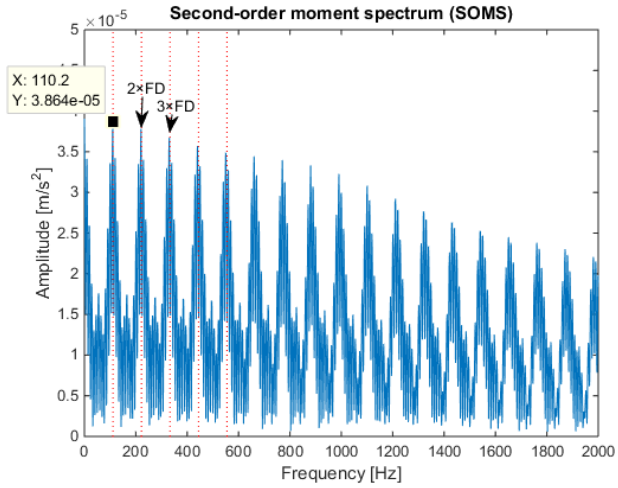

Figure 7. SOMS of signal B804.

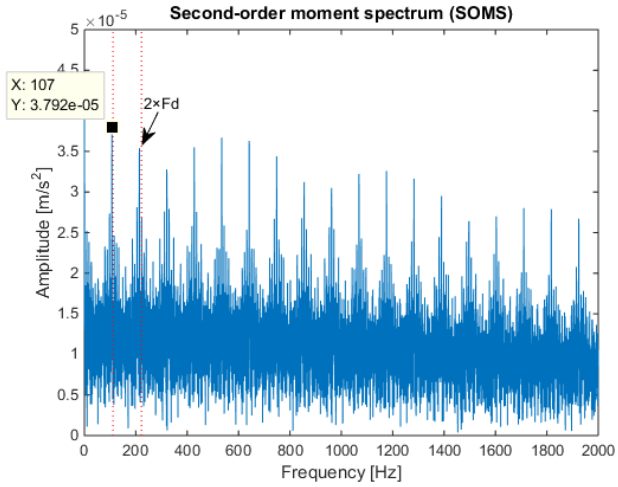

Figure 8. SOMS of signal B604.

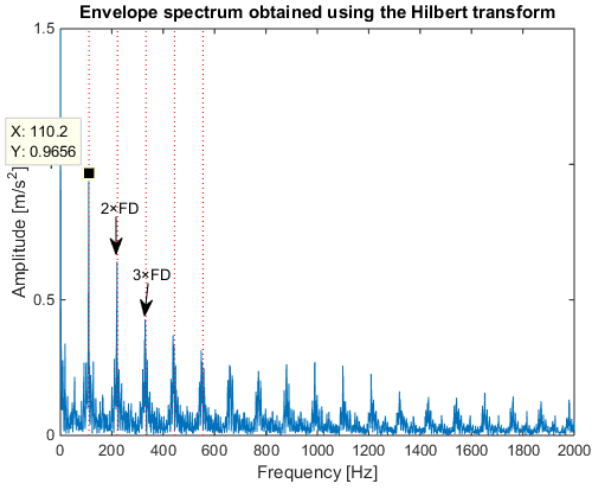

Figure 9. Envelope spectrum of signal B804.

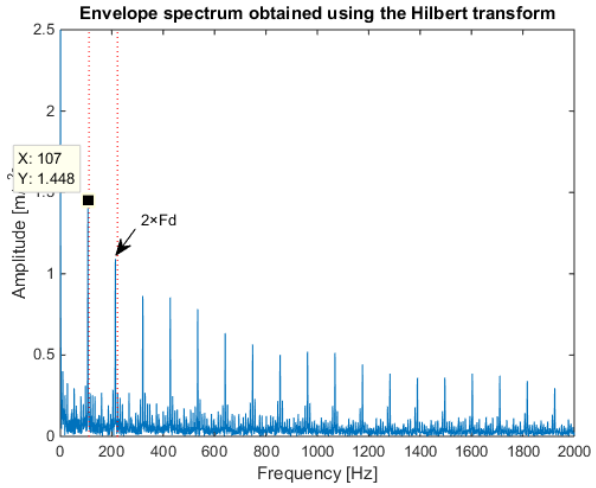

Figure 10. Envelope spectrum of signal B604.

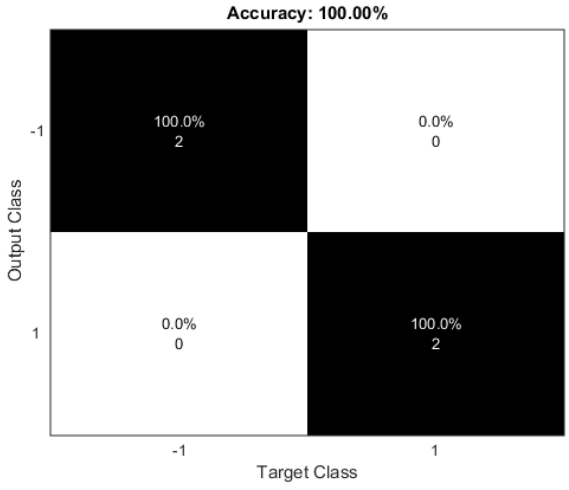

Figure 11. SVM performance.

The SVM classifier demonstrates excellent performance at 100%, as shown in the confusion matrix (Figure 11). Therefore, the parameters presented in Table 1 prove to be highly effective in defining the type of methods used in signal demodulation.

4. COMPARATIVE ANALYSIS

In this section, we illustrate a comparison between the proposed method and the defect detection method based on demodulation, known as envelope analysis. Envelope analysis, as described in references [14], [26], [27], [28], [29], comprises the following steps:

- Selection of an effective frequency band containing fault data typically involves methods like the kurtogram. However, in this particular step, we employ the CFFsgram method, the procedural details of which can be found in reference [14].
- Band-pass filtering: The two pass frequencies of this filter are determined in the initial step and are set equal to the initial and final values of the effective frequency interval.
- Fault detection via envelope spectrum or square envelope spectrum, as defined by equations (14) and (20).

$$SE(t) = E_n(t)^2 , \tag{20}$$

where: SE denotes a square envelope.

The envelope analysis is applied to the signal (B804), contingent upon the bearing ball defect 6208, as depicted in Table 3. Following application, the CFFsgram figure portrays a frequency centred at 400 Hz with a frequency bandwidth (Bw) of 800 Hz. Hence, based on the centre frequency and bandwidth,

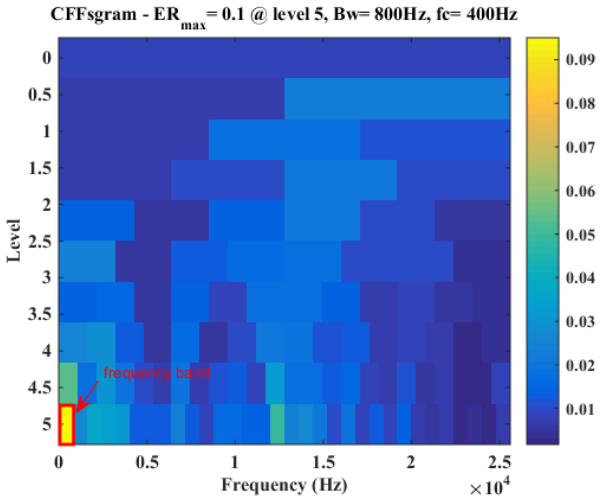

Figure 12. CFFsgram.

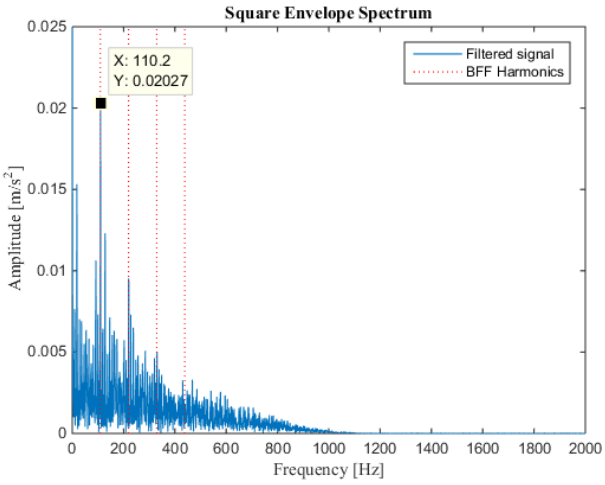

Figure 13. Square envelope spectrum.

the two filter pass frequencies are set to 0 Hz and 800 Hz, as illustrated in Figure 12. Furthermore, the square envelope spectrum depicts high-amplitude peaks at the ball defect frequency, as depicted in Figure 13. This outcome aligns identically with the findings of the proposed method.

5. CONCLUSIONS

The vibration signals, which correspond to defects in the bearing's inner ring and balls, have been extracted from the CWRU and HUST databases, respectively. They are analysed to validate and assess the second-order moment spectrum with adaptive time-varying morphological filtering, which is utilized in a defect detection method. The second-order moment spectrum is intended to streamline the shape of the spectrum, which includes sidebands, while adaptive time-varying morphological filtering is employed to eliminate noise and extract pulses from the signals. A comparison is made between the envelope spectrum obtained through the Hilbert transform and the second-order moment spectrum, followed by a classification of the characteristics of each method using the SVM classifier. Comparison of the results obtained for all the analysed signals reveals that the SOMS method effectively locates faulty bearing components based on the frequency of high-amplitude peaks. These peaks correspond to the theoretical fault frequencies of the bearing components, as defined by mathematical equations incorporating the bearing's geometric parameters and rotational speed.

Hence, the second-order moment spectrum yields results identical to those obtained with the envelope spectrum and the squared envelope spectrum, resulting in a high-amplitude peak at the fault frequency. Furthermore, the calculated statistical parameters enable us to discern the method type used, whether SOMS or the envelope determined by the Hilbert transform. SOMS is derived from mean and standard deviation formulas that rely on the original vibration signal, while the envelope spectrum is defined by the Hilbert transform, which entails a convolution operation.

ACKNOWLEDGEMENT

We thank Case Western Reserve University (CWRU) and Hanoi University of Science and Technology (HUST) for providing open access data.

REFERENCES

[1] D. Neupane, J. Seok, Bearing fault detection and diagnosis using case western reserve university dataset with deep learning approaches: A review, IEEE Access 8 (2020), pp. 93155-93178. DOI: 10.1109/ACCESS.2020.2990528

[2] K. Bouaouiche, Y. Menasria, D. Khalifa, Detection of defects in a bearing by analysis of vibration signals, Diagnostyka 24 (2023). DOI: 10.29354/diag/162230

[3] Y. Wang, J. Xiang, R. Markert, M. Liang, Spectral kurtosis for fault detection, diagnosis and prognostics of rotating machines: A review with applications, Mechanical Systems and Signal Processing 66 (2016), pp. 679-698. DOI: 10.1016/j.ymssp.2015.04.039

[4] K. Bouaouiche, Y. Menasria, D. Khalfa, Diagnosis of rotating machine defects by vibration analysis, Acta IMEKO 12 (2023) 1, pp. 1-6. DOI: 10.21014/actaimeko.v12i1.1438

[5] B. Peng, Y. Bi, B. Xue, M. Zhang, S. Wan, A survey on fault diagnosis of rolling bearings, Algorithms 15.10 (2022), pp. 347. DOI: 10.3390/a15100347

[6] Nazari, Mojtaba, Sayed Mahmoud Sakhaei. Successive variational mode decomposition, Signal Processing 174 (2020): 107610. DOI: 10.1016/j.sigpro.2020.107610

[7] Nazari, Mojtaba, Sayed Mahmoud Sakhaei. Variational mode extraction: A new efficient method to derive respiratory signals from ECG, IEEE journal of biomedical and health informatics 22.4 (2017), pp. 1059-1067. DOI: 10.1109/JBHI.2017.2734074

[8] W. Zhou, Z. Feng, X. Wang, H. Lv, Empirical fourier decomposition, arXiv preprint arXiv:1912.00414 (2019). DOI: 10.48550/arXiv.1912.00414

[9] Albezzawy, Muhammad N., Mohamed G. Nassef, Nader Sawalhi. Rolling element bearing fault identification using a novel three-step adaptive and automated filtration scheme based on Gini index, ISA transactions 101 (2020), pp. 453-460. DOI: 10.1016/j.isatra.2020.01.019

[10] Bouaouiche, Karim, Yamina Menasria, Dalila Khalfa. Detection and diagnosis of bearing defects using vibration signal processing, Archive of Mechanical Engineering 70.3 (2023), pp. 433–452. DOI: 10.24425/ame.2023.146849

[11] M. Feldman, Hilbert transform in vibration analysis, Mechanical systems and signal processing 25.3 (2011), pp. 735-802. DOI: 10.1016/j.ymssp.2010.07.018

[12] X. Shi, Z. Zhang, Z. Xia, B. Li, X. Gu, T. Shi, Application of Teager–Kaiser Energy Operator in the Early Fault Diagnosis of Rolling Bearings, Sensors 22.17 (2022): 6673. DOI: 10.3390/s22176673

[13] J. Antoni, Fast computation of the kurtogram for the detection of transient faults, Mechanical Systems and Signal Processing 21.1 (2007), pp. 108-124. DOI: 10.1016/j.ymssp.2005.12.002

[14] N. Zhou, Y. Cheng, Z. Wang, B. Chen, W. Zhang, CFFsgram: A candidate fault frequencies-based optimal demodulation band selection method for axle-box bearing fault diagnosis, Measurement 207 (2023): 112368. DOI: 10.1016/j.measurement.2022.112368

[15] Y. Miao, B. Zhang, J. Lin, M. Zhao, H. Lui, Z, Liu, H. Li, A review on the application of blind deconvolution in machinery fault diagnosis, Mechanical Systems and Signal Processing 163 (2022): 108202. DOI: 10.1016/j.ymssp.2021.108202

[16] C. A. Cabrelli, Minimum entropy deconvolution and simplicity; a noniterative algorithm, Geophysics 50.3 (1985): 394-413. DOI: 10.1190/1.1441919

[17] G. L. McDonald, Qing Zhao, Ming J. Zuo. Maximum correlated Kurtosis deconvolution and application on gear tooth chip fault detection, Mechanical Systems and Signal Processing 33 (2012), pp. 237-255. DOI: 10.1016/j.ymssp.2012.06.010

[18] M. Buzzoni, J. Antoni, G. d'Elia. Blind deconvolution based on cyclostationarity maximization and its application to fault identification, Journal of Sound and Vibration 432 (2018): 569-601. DOI: 10.1016/j.jsv.2018.06.055

[19] Z. Wang, J. Zhou, W. Du, Y. Lei, J. Wang, Bearing fault diagnosis method based on adaptive maximum cyclostationarity blind deconvolution, Mechanical Systems and Signal Processing 162 (2022): 108018. DOI: 10.1016/j.ymssp.2021.108018

[20] Thuan, Nguyen Duc, Hoang Si Hong. HUST bearing: a practical dataset for ball bearing fault diagnosis, BMC research notes 16.1 (2023): 138. DOI: 10.1186/s13104-023-06400-4

[21] B. Chen, D. Song, W. Zhang, Y. Cheng, Z. Wang, A performance enhanced time-varying morphological filtering method for bearing fault diagnosis, Measurement 176 (2021): 109163. DOI: 10.1016/j.measurement.2021.109163

[22] T. Han, L. Zhang, Z. Yin, A. C. C. Tan, Rolling bearing fault diagnosis with combined convolutional neural networks and support vector machine, Measurement 177 (2021): 109022.

DOI: 10.1016/j.measurement.2021.109022
[23] A. Widodo, B.-S. Yang. Support vector machine in machine condition monitoring and fault diagnosis, Mechanical systems and signal processing 21.6 (2007), pp. 2560-2574.
DOI: 10.1016/j.ymssp.2006.12.007
[24] Roy, Sayanjit Singha, Sayantan Dey, Soumya Chatterjee. Autocorrelation aided random forest classifier-based bearing fault detection framework, IEEE Sensors Journal 20.18 (2020), pp. 10792-10800.
DOI: 10.1109/JSEN.2020.2995109
[25] Case Western Reserve University, Bearing Data center. Online [Accessed 10 November 2023] https://engineering.case.edu/bearingdatacenter.
[26] B. Hou, Y. Chen, H. Wang, Z. Peng, K.-L. Tsui, D. Wang, OSESgram: Data-aided method for selection of informative frequency bands for bearing fault diagnosis, IEEE transactions on instrumentation and measurement 71 (2022), pp. 1-10.
DOI: 10.1109/TIM.2022.3175037
[27] T. Chen, L. Guo, T. Feng, H. Gao, Y. Yu, IESMGCFFOgram: A new method for multicomponent vibration signal demodulation and rolling bearing fault diagnosis, Mechanical Systems and Signal Processing 204 (2023): 110800.
DOI: 10.1016/j.ymssp.2023.110800
[28] X. Wang, J. Zheng, Q. Ni, H. Pan, J. Zhang, Traversal index enhanced-gram (TIEgram): A novel optimal demodulation frequency band selection method for rolling bearing fault diagnosis under non-stationary operating conditions, Mechanical Systems and Signal Processing 172 (2022): 109017.
DOI: 10.1016/j.ymssp.2022.109017
[29] Chen, Xin, Yu Guo, Jing Na. Improvement on IESFOgram for demodulation band determination in the rolling element bearings diagnosis, Mechanical Systems and Signal Processing 168 (2022): 108683.
DOI: 10.1016/j.ymssp.2021.108683